# Light transmission from a twisted nematic liquid crystal: Accurate methods to measure the azimuthal anchoring energy

S. Faetti* and G. C. Mutinati
*INFM and Dipartimento di Fisica, Universita di Pisa via Buonarroti 2, 56127 Pisa, Italy*
(Received 22 January 2003; published 6 August 2003)

In this paper, we analyze the light transmission from a twisted nematic liquid crystal (NLC) and we propose two accurate and very direct optical methods to measure the azimuthal anchoring energy. In both of them, a monochromatic beam of wavelength $\lambda$ with a polarization vector that rotates at an angular frequency $\omega$ impinges on a twisted nematic liquid crystal. The intensity of the transmitted beam is modulated at angular frequency $2\omega$ with a phase shift $\beta$, which is related to the surface azimuthal director angle $\phi_1$ at the investigated interface. It is shown that there exists a special geometry where the simple adiabatic relation $\phi_1 = \beta/2$ is satisfied up to second order in the small perturbative parameter $\alpha = \lambda/(2\pi\Delta n\xi)$, where $\Delta n$ is the anisotropy of the refractive indices of the NLC and $\xi$ is the twist distortion length. Furthermore, the small residual higher order correction terms can be greatly reduced by choosing a proper geometry for the experiment. With this choice, the range of validity of the adiabatic theory is greatly extended. The perturbative theoretical results are fully confirmed by numerical calculations. The azimuthal anchoring energy coefficient can be obtained by measuring phase shift $\beta$ versus the intensity of an applied magnetic field. These methods greatly improve the accuracy of the previous transmitted light techniques and also provide accurate measurements of strong azimuthal anchoring energies.

DOI: 10.1103/PhysRevE.68.026601 PACS number(s): 61.30.Hn, 42.70.−a, 61.30.Gd, 78.20.Ci

## I. INTRODUCTION

The macroscopic behavior of nematic liquid crystals (NLC) is described by the unit vector field $\mathbf{n}(\mathbf{r})$ which is called the *director* [1]. $\mathbf{n}(\mathbf{r})$ represents the local average orientation of the long molecular axes. The surface alignment $\mathbf{n_s}$ of the director is determined by the competition between surface and bulk interactions. $\mathbf{n_s}$ is characterized by the surface polar angle $\theta_s$ that the director makes with axis $z$ orthogonal to the surface and the surface azimuthal angle $\phi_s$ that the director makes with axis $x$ in the surface plane (see Fig. 1).

In the absence of external torques, the director is aligned along the direction (*easy axis*) that minimizes the anchoring energy $W(\mathbf{n_s})$ [1,2]. $W(\mathbf{n_s})$ represents the work needed to rotate the director from the easy axis toward the actual surface orientation. If $\theta_s$ is held fixed and equal to the easy polar angle $\theta_e$, $W(\theta_s,\phi_s)$ becomes a function of $\phi_s$ only, which is called the *azimuthal anchoring energy*. Different experimental methods have been used to measure the azimuthal anchoring energy. Most of them consist in the optical measurement of the polarization state of either transmitted [3–13] or reflected [14–16] light. In all these cases, a known torque is applied on the director and the consequent rotation of the director at the surface is measured. The torque can be generated either by applying external fields (magnetic or electric) or exploiting the competition between different surface orientations (hybrid cell [10]).

In a typical transmission experiment, the polarization of a monochromatic beam, which is transmitted through a nematic layer, is measured. From this measurement, the surface azimuthal angle can be obtained. The calculation of the dependence of the polarization of the transmitted light on the surface azimuthal angles requires a somewhat complex numerical analysis based on the Berreman transmission matrix [17]. This needs a complex fitting procedure to obtain the surface angles from the experimental results [8]. The uncertainty on the bulk material constants of the NLC and on the thickness of the nematic layer limit the applicability of this method to relatively weak anchoring energies.

The theoretical analysis of the experimental data becomes much simpler if the characteristic length $\xi$ of the bulk twist distortion is much greater than the optical wavelength $\lambda$ (the Mauguin regime). In such a case, if the polarization plane of the incident beam is parallel to the orientation of the director at the first solid-nematic interface, it remains parallel to the local director field everywhere. Then, the polarization plane of the outgoing transmitted beam is parallel to the director orientation at the second interface. This theoretical result, which is known as the *adiabatic theorem*, suggests a simple

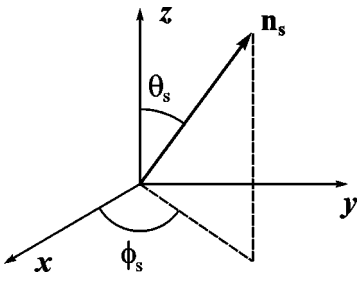


FIG. 1. Orientation of the director at the interface ($z=0$) between a nematic liquid crystal and an isotropic medium. $\phi_s$ and $\theta_s$ are the azimuthal and the polar angles of the director, respectively. $z$ is the axis orthogonal to the interface and $x$ and $y$ are two orthogonal axes on the surface plane.

*Corresponding author. Electronic address: faetti@df.unipi.it

 

experimental method to measure the surface azimuthal angles: the nematic layer is inserted between two polarizers that are rotated until the intensity of the transmitted light vanishes. This occurs when the transmission axis of the first polarizer is parallel to the director orientation at the first surface and the analyzer is orthogonal to that at the second interface. Such a method has been often used in literature (see, for instance, Ref. [3]) to measure the azimuthal anchoring energy. However, it provides accurate results only in the special case of extremely weak anchoring energies, where condition $\xi \gg \lambda$ can be fulfilled. In fact, Oldano *et al.* [5–7] showed that the adiabatic theorem corresponds to the zero order expansion of the Berreman matrix in the perturbative parameter $\alpha = \lambda/(2\pi\Delta n\xi)$, where $\Delta n = n_e - n_o \approx 0.2$ is the anisotropy of the refractive indices of the NLC. They showed that the first order correction is not negligible in most practical situations and simulates a spurious surface rotation of the director, which depends strongly on phase shift $\delta = 2\pi(n_e - n_o)d/\lambda$ between the extraordinary and ordinary optical beams. The first order correction is maximum if $\delta$ is an even multiple of $\pi$, but vanishes if $\delta$ is an odd multiple of $\pi$. Therefore, in order to reduce greatly these spurious contributions, they measured the surface director angle by setting the temperature of the NLC layer in such a way as to satisfy condition $\delta = m\pi$, where $m$ is an odd integer. Although this choice greatly improves the accuracy of the experimental results, the achievement of condition $\delta = m\pi$ makes the experimental procedure somewhat heavy. In particular, an accurate thermostatation of the NLC and an accurate measurement of the optical dephasing $\delta$ are needed. Furthermore, the measurement of the azimuthal anchoring energy can be performed only at those special temperatures where condition $\delta = m\pi$ is fulfilled.

More recently, Adrienko *et al.* [11] proposed a different method with a twisted nematic layer subjected to a weak external magnetic field. In such a case, the first order nonadiabatic terms proportional to $\alpha$ were taken into account in the analysis of the experimental results. This method can be applied satisfactorily only to substrates with a relatively weak anchoring energy ($W < 10^{-2}$ erg/cm$^2$).

A special behavior occurs if the director twist is produced by the competition between two different orientations of the easy axes on the two plane surfaces of the NLC layer. According to Polossat and Dozov [10], the bissectrice of the two surface easy axes is a twofold symmetry axis. Exploiting this exact symmetry, they proposed a simple transmitted light method that is virtually exact because it does not make use of any adiabatic approximation. The main drawback of this technique is that it requires that the anchoring at the investigated surface be much lower than that at the counterplate. Therefore, only moderately strong anchoring energies can be accurately measured with this technique ($W \approx 10^{-2} - 10^{-3}$ erg/cm$^2$).

In this paper, we analyze in detail the light transmission from a twisted nematic sample using both a perturbative approach and an numerical analysis. We show that there is a special geometry where the first order nonadiabatic contributions (linear terms in $\alpha$) vanish *for all values of the optical dephasing* $\delta$. Furthermore, the output signal depends only on the director azimuthal angle at interface 1 (see Fig. 2), which is first encountered by the incident beam. Then, *no assumption is needed as far as the anchoring at the second interface is concerned*. These theoretical results have been obtained using the Oldano perturbative approach and have been fully confirmed by the numerical integration of the Berreman equations. Furthermore, the numerical calculations show that the higher order contributions can also be greatly reduced with the choice of a proper experimental geometry. As a consequence of these theoretical results, we propose here two transmitted light methods (methods I and II) that provide simple and accurate measurements of the azimuthal anchoring energy at the investigated interface, also in the critical case of strong anchoring energies ($W \approx 1$ erg/cm$^2$). The measurement of the surface director angle is reduced to the standard measurement of phase $\beta$ of an oscillating signal. From the experimental point of view, method I is slightly more complicated than method II, because it requires that the director at the second surface of the nematic cell and the analyzer axis are aligned parallel to the magnetic field (see Fig. 2). An imperfect alignment introduces systematic errors in the experiment. On the contrary, method II does not require any special orientation of the director at interface 2 and any analyzer. This makes the experimental set up of method II much simpler and greatly limits the possible error sources. Both these methods overcome the main drawbacks of the known transmitted light methods and greatly increase the accuracy of the measurements of the azimuthal anchoring energy. In particular, the measurements can be performed at any temperature and no assumption on the anchoring at the counterplate is needed. Furthermore, strong anchoring energies can be measured. Finally, the experimental apparatus and the analysis of the experimental results is very simple.

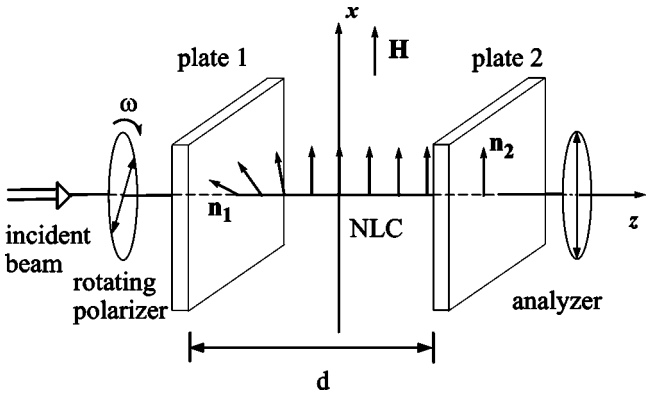


FIG. 2. Schematic view of the geometry of method I. A nematic layer of uniform thickness $d$ is sandwiched between two parallel solid plates. A magnetic field can be applied along a $x$ axis in the layer plane. The easy axis at interface 2 is parallel to the magnetic field. A monochromatic beam passes through a rotating polarizer and impinges at normal incidence on the layer. The polarization axis of the analyzer is parallel to the $x$ axis.

We believe that these experimental methods can also represent a valid alternative to the reflectometric techniques [14–16] which are known to be very accurate. In these reflectometric techniques, the surface director angle is obtained from the measurement of the polarization of a monochro-

matic optical beam which is reflected by the interface. As shown in Ref. [14], this measurement procedure is virtually unaffected by the bulk director twist but it is more sensitive to small external noise sources. In fact, the intensity of the reflected beam is two orders of magnitude lower than that of the incident beam. Therefore, relatively high power laser sources are needed ($\geqslant 10$ mW) and the actual accuracy of the measurement is appreciably affected by the noise contributions coming from the light diffused from the NLC and from other external noise contributions.

The paper is organized as follows. In Sec. II, the main aspects of the Berreman theory and of the Oldano perturbative approach are briefly discussed and a simple perturbative expression for the transmitted field is given. In Secs. III A and III B, we calculate the dephasing $\beta$ for method I, using the perturbative approach and the numerical Berreman approach, respectively. In Sec. IV A, we use the Fourier optics and the perturbative approach to calculate dephasing $\beta$, which corresponds to method II. Numerical calculations are given in Sec. IV B. Section V is devoted to the discussion of the experimental procedure that has to be used to measure the azimuthal anchoring energy. Some preliminary experimental results are also given. Section VI is devoted to conclusions.

## II. TRANSMISSION OF A MONOCHROMATIC BEAM IN A TWISTED NLC

A powerful matrix approach to the study of the transmission and the reflection from a layered anisotropic medium was proposed many years ago by Berreman [17]. Consider a plane electromagnetic wave of wavelength $\lambda$, which propagates along the $z$ axis in the positive versus and incides normally on a twisted nematic layer having the surfaces at $z=-d/2$ and $z=d/2$ as shown in Fig. 2. The director field lies everywhere in the layer plane $x$-$y$ and is given by $\mathbf{n}=[\cos\phi(z),\sin\phi(z),0]$, where $\phi(z)$ is the local director angle with the $x$ axis. We indicate by $E_x$ and $E_y$ the $x$ and $y$ components of the electric field amplitude of the electromagnetic wave and by $H_x$ and $H_y$ the corresponding magnetic field amplitudes. The electromagnetic field in any point of the nematic slab is described by the four components vector $\mathbf{\Psi}(z)=(E_x,H_y,E_y,-H_x)$. Consider now a very thin layer of thickness $h \ll \lambda$ inside the nematic LC. For sufficiently small values of $h$, the director orientation is virtually uniform in this thin layer. According to Berreman, $\mathbf{\Psi}(z+h)$ is given by

$$\mathbf{\Psi}(z+h)=\overline{\mathbf{P}}(z,h)\mathbf{\Psi}(z), \tag{1}$$

where $\overline{\mathbf{P}}(z,h)$ is the $4\times 4$ transmission matrix across the thin layer of thickness $h$, which is given by

$$\overline{\mathbf{P}}(z,h)=\exp[i2\pi h\overline{\mathbf{\Delta}}(z)/\lambda], \tag{2}$$

where matrix $\overline{\mathbf{\Delta}}(z)$ depends on the extraordinary and ordinary refractive indices $n_e$ and $n_o$ of the NLC and on the director azimuthal angle $\phi(z)$ (see Eq. (23) in Ref. [17]).

From a numerical point of view, it can be convenient to calculate $\overline{\mathbf{P}}(z,h)$ using the truncated Taylor expansion

$$\overline{\mathbf{P}}(z,h)=1+i(2\pi h/\lambda)\overline{\mathbf{\Delta}}(z)-(2\pi h/\lambda)^2\overline{\mathbf{\Delta}}(z)\overline{\mathbf{\Delta}}(z)/2+\cdots. \tag{3}$$

The output vector $\mathbf{\Psi}(d/2)$ is related to $\mathbf{\Psi}(-d/2)$ by the following relation:

$$\mathbf{\Psi}(d/2)=\overline{\mathbf{F}}(d/2,-d/2)\mathbf{\Psi}(-d/2), \tag{4}$$

where $\overline{\mathbf{F}}(d/2,-d/2)$ is given by

$$\overline{\mathbf{F}}(d/2,-d/2)=\overline{\mathbf{P}}(d/2-h,h)\overline{\mathbf{P}}(d/2-2h,h)\cdots\overline{\mathbf{P}}(-d/2,h). \tag{5}$$

Once $\overline{\mathbf{F}}(d/2,-d/2)$ is calculated, the amplitudes of the transmitted and of the reflected beams can be obtained using the procedures discussed in Ref. [17]. All the numerical calculations reported in the present paper have been performed using a Taylor expansion of $\overline{\mathbf{P}}(z,h)$ [see Eq. (3)] up to sixth order, which ensures a rapid convergence and a satisfactory accuracy of the numerical results.

Some years ago, Oldano *et al.* [5–7] proposed a perturbative approach to describe the light transmission in a twisted nematic layer subjected to a magnetic field of intensity $H$. The perturbative parameter of the theory is

$$\alpha=\lambda/(2\pi\Delta n\xi), \tag{6}$$

where $\xi$ is the magnetic coherence length

$$\xi=\sqrt{\frac{K_{22}}{\chi_a}}\frac{1}{H}. \tag{7}$$

$K_{22}$ is the twist elastic constant and $\chi_a$ is the anisotropy of the magnetic susceptibility. Disregarding the coupling between transmitted and reflected waves, the transmitted electric field can be described using a $2\times 2$ matrix Jones approach. The equations for the transmitted field are written in a rotating reference system where the $x$ and $y$ axes remain everywhere parallel and orthogonal to the local director axis. Then, the two base vectors represent the extraordinary and the ordinary electric fields, respectively. The amplitudes of the extraordinary and of the ordinary base electric fields $\mathbf{b}_e$ and $\mathbf{b}_o$ are not unitary but are chosen in such a way that the ordinary and the extraordinary waves have the same intensity. This means that $\mathbf{b}_e$ and $\mathbf{b}_o$ are proportional to $1/\sqrt{n_e}$ and $1/\sqrt{n_o}$, respectively. Disregarding the reflections at the interfaces, the $2\times 2$ transmission Jones matrix at the first order in the perturbative parameter $\alpha$ reduces to [5–7]

$$\overline{\mathbf{T}}(d/2,-d/2)=\exp(ik_a d)\begin{bmatrix}\exp(i\delta/2) & it\\ it^* & \exp(-i\delta/2)\end{bmatrix}, \tag{8}$$

where symbol * denotes complex conjugation and $t$ is the small perturbative parameter [18]:

$$t=-i\eta_1\int_{-d/2}^{d/2}\exp(-i\Delta kz)\frac{d\phi}{dz}dz, \tag{9}$$

where $k_a=\pi(n_e+n_o)/\lambda$ is the average wave vector, $\delta=\Delta kd=2\pi(n_e-n_o)d/\lambda$ is the optical dephasing between the extraordinary and the ordinary beams, and $\eta_1=[\sqrt{(n_e/n_o)}+\sqrt{(n_o/n_e)}]/2\approx 1$. By successive integrations by parts, Eq. (9) can be written in the following form:

$$t=\frac{\eta_1}{\Delta k}\left(\exp(-i\Delta kz)\frac{d\phi}{dz}\bigg|_1^2-\frac{i}{\Delta k}\times\exp(-i\Delta kz)\frac{d^2\phi}{dz^2}\bigg|_1^2+\cdots\right). \tag{10}$$

Since $d\phi/dz\approx\Delta\phi/\xi$ and $d^2\phi/dz^2\approx\Delta\phi/\xi^2$, only the first contribution in Eq. (10) is of the first order in $\alpha=\lambda/(2\pi\Delta n\xi)=1/(\Delta k\xi)$. Then, at the first order of approximation, $t$ in Eq. (10) reduces to

$$t=\frac{\eta_1}{\Delta k}\left[\exp\left(\frac{-i\Delta kd}{2}\right)\frac{d\phi}{dz}\bigg|_2-\exp\left(\frac{i\Delta kd}{2}\right)\frac{d\phi}{dz}\bigg|_1\right], \tag{11}$$

where $(d\phi/dz)|_1$ and $(d\phi/dz)|_2$ are the derivatives of the director angle at surface $1(z=-d/2)$ and $2(z=d/2)$, respectively. If thickness $d$ is much greater than $\xi$, the semi-infinite sample approximation for the director field is very well satisfied and the two surface derivatives in Eq. (11) are given by [1]:

$$\frac{d\phi}{dz}\bigg|_2=\frac{\sin\phi_2}{\xi}, \tag{12}$$

$$\frac{d\phi}{dz}\bigg|_1=-\frac{\sin\phi_1}{\xi}, \tag{13}$$

where $\phi_1$ and $\phi_2$ denote the surface azimuthal angles at surface 1 and 2, respectively. From Eqs. (8) and (11), we get

$$\overline{\mathbf{T}}(d/2,-d/2)=\begin{vmatrix}\exp(i\delta_e) & i[a\exp(i\delta_e)+b\exp(i\delta_o)]\\ i[a\exp(i\delta_o)+b\exp(i\delta_e)] & \exp(i\delta_o)\end{vmatrix}, \tag{14}$$

where $\delta_e=2\pi n_ed/\lambda$ and $\delta_o=2\pi n_od/\lambda$ are the optical dephasing of the extraordinary and the ordinary rays, and $a$ and $b$ are two small parameters defined as

$$a=-\frac{\eta_1}{\Delta k}\frac{d\phi}{dz}\bigg|_1 \tag{15}$$

and

$$b=\frac{\eta_1}{\Delta k}\frac{d\phi}{dz}\bigg|_2. \tag{16}$$

We denote by $\mathbf{n}_1$ and $\mathbf{h}_1$ two versors (in the layer plane) parallel and orthogonal to the director at surface 1 and by $\mathbf{n}_2$ and $\mathbf{h}_2$ two versors parallel and orthogonal to the director at surface 2. Amplitude $\mathbf{E}^{inc}$ of the incident field at $z=-d/2$ can be written in a compact form as

$$\mathbf{E}^{inc}=E_e^{inc}\mathbf{n}_1+E_o^{inc}\mathbf{h}_1, \tag{17}$$

where $E_e^{inc}$ and $E_o^{inc}$ are the amplitudes of the extraordinary and the ordinary components of the incident electric field, respectively. Using Eq. (14) and taking into account that base vectors $\mathbf{b}_e$ and $\mathbf{b}_o$ are proportional to $1/\sqrt{n_e}$ and $1/\sqrt{n_o}$ ($\mathbf{b}_e\propto\mathbf{n}/\sqrt{n_e}$ and $\mathbf{b}_o\propto\mathbf{h}/\sqrt{n_o}$), we obtain the following output electric field $\mathbf{E}^{out}$ at $z=d/2$:

$$\mathbf{E}^{out}=\mathbf{E}_e^{out}\exp(i\delta_e)+\mathbf{E}_o^{out}\exp(i\delta_o), \tag{18}$$

where

$$\mathbf{E}_e^{out}=(E_e^{inc}+ia\sqrt{n_o/n_e}E_o^{inc})\mathbf{n}_2+ib\sqrt{n_e/n_o}E_e^{inc}\mathbf{h}_2 \tag{19}$$

and

$$\mathbf{E}_o^{out}=ib\sqrt{n_o/n_e}E_o^{inc}\mathbf{n}_2+(E_o^{inc}+ia\sqrt{n_e/n_o}E_e^{inc})\mathbf{h}_2. \tag{20}$$

Equations (18)–(20) represent the fundamental result of the perturbative theory. Equation (18) shows that the electromagnetic signal propagates in the twisted NLC as the superposition of two waves, the generalized "*extraordinary*" wave ($\mathbf{E}_e^{out}$) and the generalized "*ordinary*" wave ($\mathbf{E}_o^{out}$) having phase velocities $c/\sqrt{n_e}$ and $c/\sqrt{n_o}$, respectively. In the adiabatic limit ($a=0$ and $b=0$), the extraordinary and the ordinary electric fields in Eqs. (19) and (20) are reduced to the standard extraordinary and ordinary waves. In particular, the corresponding electric fields are parallel and orthogonal to the local director field. For nonvanishing values of $a$ and $b$, a part of the extraordinary incident field propagates with the ordinary phase velocity and vice versa. Furthermore, an incident extraordinary (or ordinary) field does not follow exactly the rotation of the director field. In the following section we will show that it is possible to choose a proper geometry where the linear perturbative contributions vanish. Therefore, with this special geometry the range of validity of the adiabatic theorem is greatly extended.

## III. METHOD I: THEORETICAL ANALYSIS

### A. The perturbative analysis

Here we consider the geometry which corresponds to method I. An incident beam passes through a polarizer which rotates with angular frequency $\omega$ and impinges at normal incidence on a nematic liquid crystal layer. A magnetic field $\mathbf{H}$ can be applied parallel to the $x$ axis in the layer plane (see Fig. 2). The extraordinary and ordinary components of the incident field amplitude $\mathbf{E}^{inc}$ are:

$$E_e^{inc}=E_0\cos(\omega t-\phi_1) \tag{21}$$

and

$$E_o^{inc}=E_0\sin(\omega t-\phi_1), \tag{22}$$

where $E_e^{inc}=\mathbf{E}^{inc}\cdot\mathbf{n}_1$ and $E_o^{inc}=\mathbf{E}^{inc}\cdot\mathbf{h}_1$ and where the polarizer axis has been assumed to be parallel to the magnetic field ($x$ axis) at time $t=0$. An analyzer with polarization axis $\hat{\mathbf{A}}$ parallel to the director at surface 2($\hat{\mathbf{A}}=\mathbf{n}_2$) is inserted after the NLC layer. The light intensity after the analyzer is

$$I_{\mathrm{I}}^{out}=a_o(\mathbf{E}^{out}\cdot\hat{\mathbf{A}})[(\mathbf{E}^{out})^*\cdot\hat{\mathbf{A}}]=a_o(\mathbf{E}^{out}\cdot\mathbf{n_2})[(\mathbf{E}^{out})^*\cdot\mathbf{n_2}], \tag{23}$$

where $a_o$ is a suitable proportionality coefficient and subscript I refers to method I. Substituting Eqs. (18)–(20) into Eq. (23) and disregarding terms of the second order in the perturbation parameter $\alpha$, we find:

$$I_{\mathrm{I}}^{out}=a_o[(E_e^{inc})^2+2b\sqrt{n_o/n_e}E_e^{inc}E_o^{inc}\sin\delta]. \tag{24}$$

In method I, the director at the second interface is parallel to the magnetic field. In this condition, it can be easily shown that the director derivative at surface 2 is zero and coefficient $b$ in Eq. (16) vanishes. Then, the output intensity in Eq. (24) becomes

$$I_{\mathrm{I}}^{out}=a_o(E_e^{inc})^2=\frac{I_o}{2}[1+\cos 2(\omega t-\phi_1)]. \tag{25}$$

Up to the second order in the perturbative parameter $\alpha=\lambda/(2\pi\Delta n\xi)$, the output intensity is modulated at angular frequency $2\omega$ with phase coefficient $\beta=2\phi_1$. Then, in this case, the surface director angle can be obtained in a very direct way from the measurement of the phase coefficient of the transmitted beam intensity, using equality $\phi_1=\beta/2$, which corresponds to the prediction of the adiabatic theorem. Note that this important theoretical result holds for any thickness and temperature of the NLC layer. It needs only that the director at surface 2 be parallel to the magnetic field. If this latter condition is not satisfied, $b$ does not vanish and Eq. (24) can be rewritten in the following equivalent form (up to the second order in $\alpha$):

$$I_{\mathrm{I}}^{out}=\frac{I_o}{2}[1+\cos 2(\omega t-\phi_1-\gamma)], \tag{26}$$

where $\gamma$ denotes a phase shift due to the twist distortion which is given by

$$\gamma=\frac{1}{2}\arctan\left(2b\sqrt{\frac{n_0}{n_e}}\sin\delta\right). \tag{27}$$

In this case, phase shift $\beta$ of the intensity signal $I_{\mathrm{I}}^{out}$ is $\beta=2(\phi_1+\gamma)$ and thus, the adiabatic theorem ($\beta=2\phi_1$) is not satisfied. Phase shift $\gamma$ in Eq. (27) mimics an apparent rotation of the director at surface $\Delta\phi_{app}=\gamma$. A more accurate expression can be obtained by taking into account the anisotropy of the ordinary and extraordinary transmission coefficients at the solid-nematic interfaces. The improved expression of $\gamma$ is

$$\gamma=\frac{1}{2}\arctan\left(2b\sqrt{\frac{n_0}{n_e}}\frac{n_e+n}{n_o+n}\sin\delta\right), \tag{28}$$

where $n$ is the refractive index of the solid substrates.

### B. Numerical calculations with the Berreman matrix

The theoretical results in Sec. III A were obtained using the first order perturbative theory. At this order of approximation, the simple adiabatic result $\phi_1=\beta/2$ remains satisfied, provided that the director at surface 2 is set parallel to the magnetic field. With this choice the validity range of the adiabatic theorem is greatly extended and the surface director azimuthal angle $\phi_1$ can be directly obtained from the measurement of phase $\beta$ of intensity $I_{\mathrm{I}}^{out}$. However, also in this case, some small residual corrections to the adiabatic theorem are present, coming from the higher order perturbative contributions. This means that the surface director angle, which is obtained experimentally using the adiabatic expression $\phi_1=\beta/2$, is affected by a residual uncertainty. Therefore, it is important to calculate these contributions in order to estimate the actual accuracy of the proposed method. The detailed analysis of these higher order contributions can be also useful in finding suitable geometric conditions where they are minimized. This section is devoted to the numerical calculation of the ''exact'' behavior of the transmitted beam in the twisted nematic layer. We will show that the higher order contributions lead to an additional small dephasing of intensity $I_{\mathrm{I}}^{out}(t)$, which mimics a small apparent rotation $\Delta\phi_{app}$ of the director at the surface. Furthermore, we will show that $\Delta\phi_{app}$ depends greatly on the director angle $\phi_1$ at surface 1 and vanishes if the director is orthogonal or parallel to the magnetic field. This dependence suggests that the accuracy of the measurements can be greatly improved by setting the easy axis at surface 1 almost orthogonal to the magnetic field.

The apparent rotation $\Delta\phi_{app}$ is calculated using the Berreman Matrix approach [17]. The accuracy of the numerical program is checked by comparing the numerical results with the exact expressions predicted in the limit cases $H=0$ and $H\rightarrow\infty$. These limit cases are recovered with a relative accuracy better than $10^{-9}$. As a further control, we calculate the sum of the transmitted and reflected intensities and we compare this sum with the incident intensity. The relative differ-

ence between these quantities is found always lower than $10^{-9}$. $\Delta\phi_{app}$ is obtained using the numerical procedure discussed below. First we calculate the transmitted electric field amplitudes $\mathbf{K}_e^{out}$ and $\mathbf{K}_o^{out}$, which correspond to an incident field of unitary amplitude polarized parallel or orthogonal to the director field at surface 1, respectively. Due to the linearity of the Berreman equations, the output field amplitude for an incident field of amplitude $E_o$ with a polarization which rotates at angular frequency $\omega$ is

$$\mathbf{E}^{out}=E_o[\mathbf{K}_e^{out}\cos(\omega t-\phi_1)+\mathbf{K}_o^{out}\sin(\omega t-\phi_1)]. \tag{29}$$

The output intensity of the transmitted beam after the analyzer is obtained by substituting $\mathbf{E}^{out}$ of Eq. (29) into Eq. (23). After straightforward calculations we get

$$I_{\mathrm{I}}^{out}=I_o\frac{a_{\mathrm{I}}+b_{\mathrm{I}}}{2}+\frac{I_o}{2}\sqrt{(a_{\mathrm{I}}-b_{\mathrm{I}})^2+c_{\mathrm{I}}^2}\cos 2(\omega t-\phi_1-\gamma), \tag{30}$$

where

$$\gamma=\frac{1}{2}\arctan\left(\frac{c_{\mathrm{I}}}{a_{\mathrm{I}}-b_{\mathrm{I}}}\right) \tag{31}$$

and $a_{\mathrm{I}}$, $b_{\mathrm{I}}$, and $c_{\mathrm{I}}$ are real numbers given by

$$a_{\mathrm{I}}=(\mathbf{K}_e^{out}\cdot\hat{\mathbf{A}})[(\mathbf{K}_e^{out})^*\cdot\hat{\mathbf{A}}], \tag{32}$$

$$b_{\mathrm{I}}=(\mathbf{K}_o^{out}\cdot\hat{\mathbf{A}})[(\mathbf{K}_o^{out})^*\cdot\hat{\mathbf{A}}], \tag{33}$$

and

$$c_{\mathrm{I}}=2\,\mathrm{Re}\{(\mathbf{K}_e^{out}\cdot\hat{\mathbf{A}})[(\mathbf{K}_o^{out})^*\cdot\hat{\mathbf{A}}]\}. \tag{34}$$

$\mathrm{Re}(\cdots)$ denotes the real part of a complex number and $\hat{\mathbf{A}}$ is the analyzer axis parallel to $\mathbf{n}_2$. $I_o$ is the intensity of the incident beam. Equation (30) reduces to Eq. (25) in the Mauguin regime since $b_{\mathrm{I}}$ and $c_{\mathrm{I}}$ vanish. Note that in the general case, the twist distortion produces both a spurious phase shift $2\gamma$ of the oscillating signal and a change of its amplitude. The phase shift mimics an apparent rotation $\Delta\phi_{app}=\gamma$ of the director at the surface. This means that the actual surface director angle $\phi_1$ does not coincide with $\beta/2$ but is given by $\phi_1=\beta/2-\Delta\phi_{app}$. Therefore, $\Delta\phi_{app}$ represents the uncertainty on the measurement of the director surface angle when the adiabatic formula $\phi_1=\beta/2$ is used.

Figure 3 shows the typical dependence of the apparent surface rotation $\Delta\phi_{app}=\gamma$ on the intensity of the magnetic field. The material parameters of the NLC used to make the numerical calculations are those of the NLC 5CB at room temperatures that are given in the caption of Fig. 3. The different full curves in Fig. 3 correspond to the apparent rotations obtained numerically for different values of the director azimuthal angle $\phi_2$ at surface 2 and for a thickness $d=235$ $\mu$m, giving an optical dephasing $\delta=140\pi+\pi/2$ (for this value of $\delta$, the first order nonadiabatic corrections have the maximum value). The broken straight lines correspond to the predictions of the first order perturbative theory

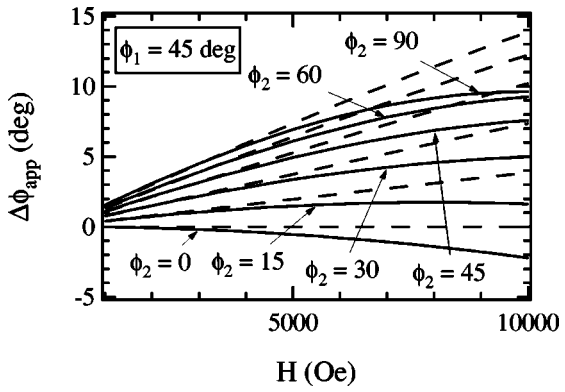


FIG. 3. Apparent rotation $\Delta\phi_{app}$ of the director at surface 1 vs intensity $H$ of the magnetic field. The full curves represent the results obtained using the numerical calculations (Berreman theory) when the director azimuthal angle at the first interface is $\phi_1=45°$. Different curves from the bottom to the top correspond to $\phi_2=0°$, $\phi_2=15°$, $\phi_2=30°$, $\phi_2=45°$, $\phi_2=60°$, $\phi_2=90°$, respectively. The broken lines represent the predictions of the first order perturbative theory [Eq. (28)]. The material parameters used to make the numerical calculations are those of the nematic liquid crystal 5CB at room temperature ($T=25$ °C): $n_e=1.717$ and $n_o=1.528$ [24], $K_{22}=3.93\times10^{-7}$ dynes [22], and $\chi_a=1.07\times10^{-7}$ [23]. The refractive index of the solid plates is $n=1.51$. The thickness of the nematic layer is $d=235$ $\mu$m which corresponds to the optical dephasing $\delta=140\pi+\pi/2$.

[$\gamma$ in Eq. (28)]. The numerical results accurately approach the predictions of the perturbative theory for sufficiently small magnetic fields ($H<2$ kOe). This confirms the validity of the theoretical expressions obtained with the perturbative approach. In the special case where $\phi_2=0°$, the apparent rotation is very small and is only due to the higher order perturbative contributions. In such a case and for $\alpha<0.28$, the apparent rotation is described very accurately (within 0.001°) by the following simple formula:

$$\Delta\phi_{app}=a_2\alpha^2+a_4\alpha^4, \tag{35}$$

where $a_2$ and $a_4$ are adimensional numerical coefficients which depend on the director surface angle $\phi_1$ and on the refractive indices of the NLC and of the substrate. $\alpha=0.28$ corresponds to the case where a magnetic field of 10 kOe is applied to a 5CB sample at room temperature.

Figure 4 shows the dependence of $\Delta\phi_{app}$ on $\alpha^2$ for some values of the director angle $\phi_1$ at surface 1 and for $\phi_2=0°$. The full lines in Fig. 4 correspond to the best fits with equation $\Delta\phi_{app}=a_2\alpha^2+a_4\alpha^4$. In this range of values of parameter $\alpha$, the quadratic contribution is the dominant one (the best fit curves in Fig. 4 are very close to straight lines). Results in Figs. 3 and 4 were obtained for a thickness $d$ of the nematic layer, which corresponds to the optical dephasing $\delta=140\pi+\pi/2$. However, for $d>6\xi$ and $\phi_2=0°$, the apparent surface rotation is virtually independent of the thickness of the nematic layer and thus, on the optical dephasing $\delta$. In particular, the maximum relative variations of $\Delta\phi_{app}$ due to changes of thickness are less than 1%. On the contrary, for $\phi_2\neq0°$, the apparent surface rotation shows

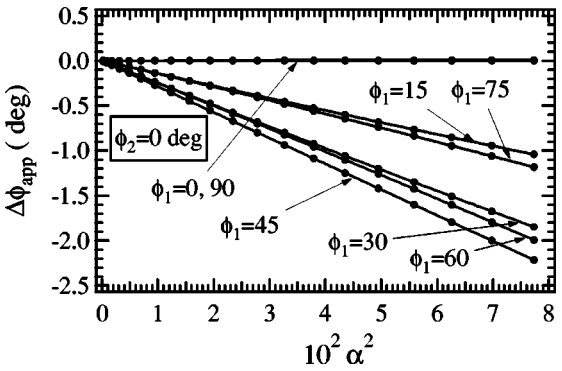


FIG. 4. $\Delta\phi_{app}$ vs the square power of the perturbative parameter $\alpha=1/(\Delta k\xi)$ defined in Eq. (6). The director angle at surface 2 is $\phi_2=0°$. The maximum value of $\alpha^2$ corresponds to magnetic field $H=10$ kOe. The points correspond to the numerical results obtained with the Berreman approach. The full curves represent the best fits with Eq. (35). Different curves correspond to the values of $\Delta\phi_{app}$ obtained when the director angles at surface 1 have the values: $\phi_1=0°$, $\phi_1=15°$, $\phi_1=30°$, $\phi_1=45°$, $\phi_1=60°$, $\phi_1=75°$, and $\phi_1=90°$. The material and geometric parameters are the same as in Fig. 3.

the $\sin\delta$ dependence predicted by the perturbative approach [see Eq. (28)]. Looking at Fig. 4, it is evident that $\Delta\phi_{app}$ depends greatly on the director angle $\phi_1$ at surface 1 and vanishes for $\phi_1=0°$ and $\phi_1=90°$, respectively. In fact, a satisfactory approximated expression for $\Delta\phi_{app}$ is given by (see Appendix A)

$$\Delta\phi_{app}=a_{21}\alpha^2\frac{\sin 2\phi_1}{2}, \tag{36}$$

where $a_{21}$ is a numerical coefficient which depends only on refractive indices $n_e$ and $n_o$ of the NLC and on refractive index $n$ of the substrate. For $n_e=1.717$, $n_o=1.528$, and $n=1.51$, we get $a_{21}=-57.3°$. Equation (36) can be used to estimate the residual uncertainty on the measurements of the surface director angle $\phi_1$ when the simple adiabatic expression $\phi_1=\beta/2$ is used. A more accurate analytical expression for $\Delta\phi_{app}$ can be found in Appendix A.

In conclusion, the predictions of the first order perturbative approach are fully confirmed by the numerical calculations. In particular, the first order corrections vanish if the geometry of method I is used ($\phi_2=0°$). A very important result of the numerical calculations is that the small residual higher order contributions also vanish when the director at surface 1 is orthogonal or parallel to the magnetic field. Therefore, in these special conditions, the adiabatic expression of phase shift $\beta$ is virtually exact for any value of the applied magnetic field. This latter results suggests that a further great improvement of the accuracy on the measurement of the surface director angle can be reached by setting the easy angle at surface 1 almost orthogonal to the magnetic field.

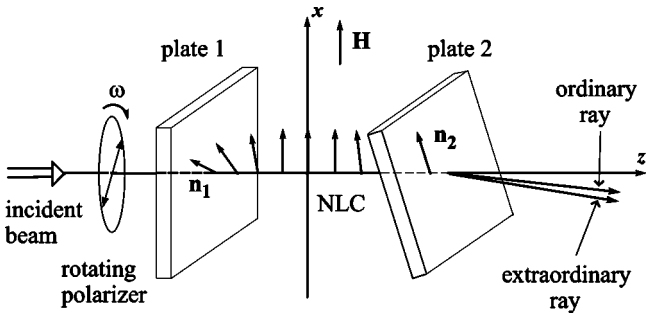


FIG. 5. Schematic view of the geometry of method II. A nematic liquid crystal wedge is inserted between two solid plates. A magnetic field can be applied along the $x$ axis parallel to surface 1. The director easy axis at surface 2 is parallel to the magnetic field. A monochromatic beam passes through a rotating polarizer and impinges on surface 1 at normal incidence. Due to the birefringence of the NLC and to the presence of the wedge, the extraordinary and the ordinary beams are spatially separated.

## IV. METHOD II: THEORETICAL ANALYSIS

### A. The perturbative analysis

Equation (18) represents the perturbative expression of the output electric field amplitude for a monochromatic beam which passes through a nematic layered sample. If the nematic sample forms a wedge with wedge angle $\theta_W \ll 1$ rad (see Fig. 5), Eq. (18) is still satisfied but the local thickness $d$ of the nematic sample becomes a linear function of the $x$ coordinate along the wedge axis

$$d=d_o+(\tan\theta_W)x\approx d_o+(\theta_W)x. \tag{37}$$

Then, the output field becomes

$$\mathbf{E}^{out}=\mathbf{E}_e^{out}\exp[i2\pi n_e(d_o+\theta_W x)/\lambda] + \mathbf{E}_o^{out}\exp[i2\pi n_o(d_o+\theta_W x)/\lambda]. \tag{38}$$

The wedge introduces two different phase modulations along the $x$ axis for the extraordinary and the ordinary optical rays. Then, according to the Fourier optics [19], these two rays are refracted at the two different angles $(n_e-1)\theta_W$ and $(n_o-1)\theta_W$, respectively, as shown schematically in Fig. 5.

In such a case, it is possible to measure separately the two corresponding intensities $I_e^{out}$ and $I_o^{out}$. The intensity of the extraordinary wave is

$$I_e^{out}=a_o[(\mathbf{E}_e^{out})\cdot(\mathbf{E}_e^{out})^*], \tag{39}$$

where $\mathbf{E}_e^{out}$ is given in Eq. (19). By substituting in Eq. (39) the expression of $\mathbf{E}_e^{out}$ given in Eq. (19), taking into account Eqs. (21) and (22) and neglecting all contributions of the second order in $\alpha$, we get

$$I_e^{out}(t)=\frac{I_o}{2}[1+\cos 2(\omega t-\phi_1)]. \tag{40}$$

Then, within the first order perturbative approach, the presence of the director twist does not introduce any additional phase shift in the oscillating signal $I_e^{out}(t)$. This is analogous

to what happened for method I in the special case $b=0$ ($\phi_2=0°$), but now this result remains satisfied for *any value* of $b$, that is, for any orientation of the director at the second interface. At this order of approximation, the phase shift in Eq. (40) depends only on the director orientation at the first interface and is completely independent of the director orientation at the other interface.

### B. Numerical calculations with the Berreman matrix

In order to verify the theoretical predictions of the perturbative approach and to obtain the higher order corrections, we have performed numerical calculations using the Berreman method. The procedure used here is a little more complicated than in the previous case, because the amplitudes of the different waves (ordinary and extraordinary) have to be separated from a proper numerical analysis, as shown in Appendix B. Using this numerical procedure, we were able to obtain the amplitude of the generalized extraordinary wave $\mathbf{E}_e^{out}$. We denote by $(\mathbf{K}_e^{out})_e$ and $(\mathbf{K}_e^{out})_o$ the numerically calculated amplitudes of the generalized extraordinary wave that correspond to an incident electric field of unitary amplitude, which is polarized parallel or orthogonal to the director at the first surface, respectively. Due to the linearity of the Berreman equations, the amplitude of the generalized extraordinary wave, which corresponds to an incident field of amplitude $E_o$ with a polarization vector which rotates with the angular velocity $\omega$, is given by

$$\mathbf{E}_{\mathrm{II}}^{out}=E_o[(\mathbf{K}_e^{out})_e\cos(\omega t-\phi_1) + (\mathbf{K}_e^{out})_o\sin(\omega t-\phi_1)]\exp(i\delta_e), \tag{41}$$

where suffix II refers to method II. Then, the intensity of the extraordinary wave in Eq. (41) is

$$I_e^{out}=I_o\frac{a_{\mathrm{II}}+b_{\mathrm{II}}}{2}+\frac{I_o}{2}\sqrt{(a_{\mathrm{II}}-b_{\mathrm{II}})^2+c_{\mathrm{II}}^2}\cos 2(\omega t-\phi_1-\gamma), \tag{42}$$

where

$$\gamma=\frac{1}{2}\arctan\left(\frac{c_{\mathrm{II}}}{a_{\mathrm{II}}-b_{\mathrm{II}}}\right) \tag{43}$$

and

$$a_{\mathrm{II}}=(\mathbf{K}_e^{out})_e\cdot(\mathbf{K}_e^{out})_e^*, \tag{44}$$

$$b_{\mathrm{II}}=(\mathbf{K}_e^{out})_o\cdot(\mathbf{K}_e^{out})_o^*, \tag{45}$$

and

$$c_{\mathrm{II}}=2\,\mathrm{Re}[(\mathbf{K}_e^{out})_e\cdot(\mathbf{K}_o^{out})_o^*]. \tag{46}$$

Equation (42) reduces to Eq. (40) in the Mauguin regime since $b_{\mathrm{II}}$ and $c_{\mathrm{II}}$ vanish. In this case too, the main effect of the bulk director twist is an apparent rotation $\Delta\phi_{app}=\gamma$.

Figure 6 shows the dependence of $\Delta\phi_{app}$ on $\alpha^2$ for $\phi_2=0°$ and $\phi_2=90°$, and with $\phi_1=45°$. Curves corresponding to $0°<\phi_2<90°$ are not shown because they lie between the two curves in the figure. This means that the higher order correction terms are poorly sensitive to the value of the director angle at surface 2.

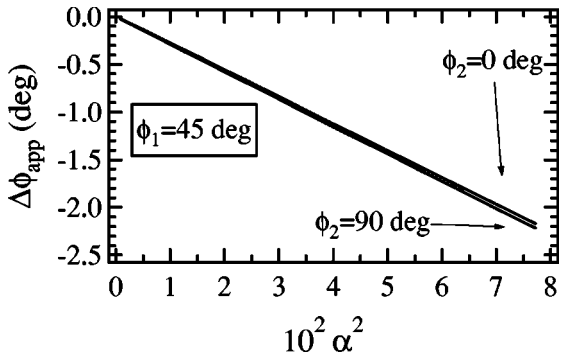


FIG. 6. Apparent rotation $\Delta\phi_{app}$ of the director at surface 1, in the case of method II, vs the square power of perturbative parameter $\alpha=1/(\Delta k\xi)$ defined in Eq. (6). The two curves in the figure from the bottom to the top represent the results obtained using the numerical calculations (Berreman theory) when the director azimuthal angle at the first interface is $\phi_1=45°$, while $\phi_2=0°$ and $\phi_2=90°$, respectively. For clarity, the curves corresponding to $0°<\phi_2<90°$ are not represented because they are internal to the two curves shown in the figure. Note that $\Delta\phi_{app}$ is poorly dependent on $\phi_2$ and is always a quadratic function of parameter $\alpha$, in agreement with the predictions of the perturbative theory. The material parameters are the same as in Fig. 3.

Figure 7 shows the dependence of $\Delta\phi_{app}$ on $\alpha^2$ for some values of $\phi_1$ and with $\phi_2=0°$. The predictions of the perturbative procedure are entirely satisfied. In particular, the apparent director rotation $\Delta\phi_{app}=\gamma$ does not show linear contributions in $\alpha$ for all values of the surface director angles $\phi_1$ and $\phi_2$. Furthermore, for $\alpha<0.28$ ($\alpha^2<0.078$ in figure) the apparent surface rotation is well represented by Eq. (35) with coefficients $a_2$ and $a_4$ that depend on the surface angle $\phi_1$ and on the refractive indices of the NLC and of the substrate, and are poorly sensitive to the value of the director angle at surface 2. Furthermore, the leading contribution,

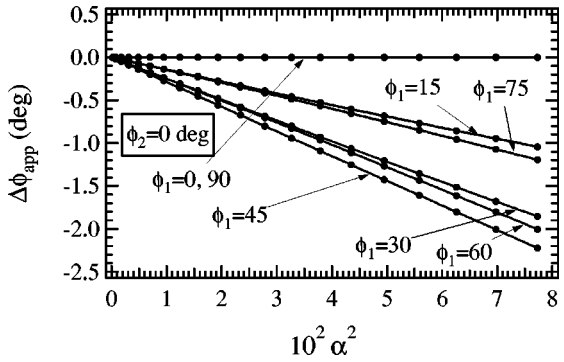


FIG. 7. $\Delta\phi_{app}$ vs the square power of the perturbative parameter $\alpha=1/(\Delta k\xi)$ defined in Eq. (6) for case $\phi_2=0°$. Different symbols correspond to the numerical "exact" values of $\Delta\phi_{app}$, obtained when the director angles at surface 1 have the values: $\phi_1=0°$, $\phi_1=15°$, $\phi_1=30°$, $\phi_1=45°$, $\phi_1=60°$, $\phi_1=75$, and $\phi_1=90°$. The full lines correspond to the best fits with Eq. (35). The material parameters are the same as in Fig. 3.

which is quadratic in $\alpha$, has the same functional dependence as in Eq. (36). More details on the higher order contributions can be found in Appendix C.

## V. MEASUREMENTS OF AZIMUTHAL ANCHORING ENERGY

In this section, the experimental procedure which we propose to obtain the azimuthal anchoring energy is discussed. Some preliminary experimental results will be given in the final part of the section. To measure the azimuthal anchoring energy of the NLC, a magnetic field **H** (or an electric field **E**) is applied along the $x$ axis (see Figs. 2 and 5) to generate a known surface elastic torque which changes the surface director azimuthal angle $\phi_1$. At equilibrium, the surface elastic torque is balanced by the anchoring restoring torque. To simplify the theoretical analysis below, we assume that the characteristic twist distortion length $\xi$ [Eq. (7)] is much smaller than the local thickness of the nematic layer so that the semi-infinite approximation can be used [1]. Furthermore, we assume that the anchoring energy function is represented by the Rapini-Papoular expression [20]. Both these assumptions are not needed but allow us to simplify the theoretical analysis. In these conditions, rotation $\Delta\phi_1$ of the surface director with respect to the easy axis satisfies the following boundary condition:

$$-\frac{\sin(\phi_e+\Delta\phi_1)}{\xi}=\frac{W}{2K_{22}}\sin(2\Delta\phi_1), \tag{47}$$

where $W$ is the anchoring energy coefficient and $\phi_e$ the easy azimuthal angle at surface 1 (with respect to the magnetic field). The left-hand side in Eq. (47) represents the surface elastic torque while the right-hand side is the restoring anchoring torque. For sufficiently small magnetic fields $[K_{22}/(W\xi)\ll 1]$, $\Delta\phi_1$ is very small and Eq. (47) is reduced to

$$\Delta\phi_1=-\frac{K_{22}}{W\xi}\sin\phi_e. \tag{48}$$

Note that for $\Delta\phi_1\ll 1$, Eq. (48) also holds in the case where the surface anchoring energy is not represented by the simple Rapini-Papoular form. Substituting the explicit expression of $\xi$ [Eq. (7)] in Eq. (48), we get the equivalent form

$$\Delta\phi_1=-\frac{\sqrt{K_{22}\chi_a}}{W}H\sin\phi_e. \tag{49}$$

In this regime, the surface director rotation is proportional to intensity $H$ of the magnetic field with a proportionality coefficient which depends on the anchoring energy coefficient $W$. Then, a simple way to obtain the anchoring energy coefficient consists on measuring the rotation angle $\Delta\phi_1$ versus the intensity $H$ of the applied magnetic field [21].

The full lines in Figs. 8(a–d) show the surface azimuthal rotation $-\Delta\phi_1=\phi_e-\phi_1$ versus intensity $H$ of the applied magnetic field for different values of the anchoring energy coefficient $W$ in the case of method I. The surface rotation has been calculated by solving the implicit equation (47) with $\xi$ given in Eq. (7). The material parameters used to make calculations are those of the nematic liquid crystal 5CB at temperature $T=25$ °C (see the figure caption in Fig. 3). The easy axis of surface 1 is $\phi_e=89°$. The full curves correspond to the exact values of the surface director rotation $-\Delta\phi_1$, while the points correspond to the values of the rotation angle which is obtained using the first order approximated expression $\Delta\phi_1=\Delta\beta/2$. According to Eq. (49), all the full curves are well represented by a straight line for small enough magnetic fields. For weak anchoring energies [$W\leqslant 10^{-3}$ erg/cm$^2$ in Fig. 8(a)], the discrepancy between the exact and the approximated ($-\Delta\beta/2$) results is completely negligible (below 1%) in the whole range of magnetic fields. For $W\geqslant 3\times 10^{-3}$ erg/cm$^2$, some discrepancy between exact and approximated results appears in the high magnetic field region. The difference between approximate results (points) and exact results (full lines) is just equal to $\Delta\phi_{app}$. It has to be emphasized that a satisfactory agreement between approximate (points) and exact results (full lines) is always observed for $H<2$ kOe. It is also important to emphasize that the differences between the adiabatic results and the exact ones, which are somewhat small in Figs. 8(a–d) will be extremely higher in a standard geometry where the linear nonadiabatic contributions do not vanish (see Fig. 3). Let us consider, for instance, the case of curve $W_7$ in Fig. 8(c). In this case, the maximum discrepancy between the true surface rotation and the approximated one is about 0.2°, which is about 20% of the true rotation. In this same case, the linear corrections can reach maximum values of about 8° that is about 800% of the true surface rotation. The broken lines in Figs. 8(a–d) show the values that are obtained by subtracting from $\beta/2$ the apparent rotation $\Delta\phi_{app}$ calculated analytically using Eqs. (A8) and (A9) with the numerical coefficients given in Table I. The broken lines are virtually superimposed to the full ones in Figs. 8(a–d) and small differences are visible only for somewhat strong anchoring energies [Fig. 8(d)]. Similar results have been obtained for method II.

The more important feature of our geometry is related to the fact that the spurious rotation $\Delta\phi_{app}$ is a quadratic function of the magnetic field ($\alpha^2\propto H^2$), while the true surface rotation at small magnetic fields is a linear function of the magnetic field. This suggests a very simple way to measure the anchoring energy coefficient $W$ which consists in restricting the analysis of the data to the region of magnetic fields where the experimentally measured phase shift shows a linear dependence on the intensity of the magnetic field [regions below $H=2$ kOe in Figs. 8(a–d)]. The experimental observation of a linear behavior ensures automatically that the nonlinear spurious nonadiabatic contribution $\Delta\phi_{app}$ is completely negligible (points and full lines are virtually coincident in Fig. 8 for $H<2$ kOe). Therefore, equality $\Delta\beta/2=\Delta\phi_1$ can be used to obtain the true surface director rotation. In these conditions, the anchoring energy coefficient can be obtained in a very simple way from the measurement of the proportionality coefficient between $\Delta\phi_1=\Delta\beta/2$ and $H$ [see Eq. (49)]. Some practical problem with this very simple and direct method can only occur in the special case of very strong anchoring energies [$W\approx 1$ erg/cm$^2$ in Fig. 8(d)]. In

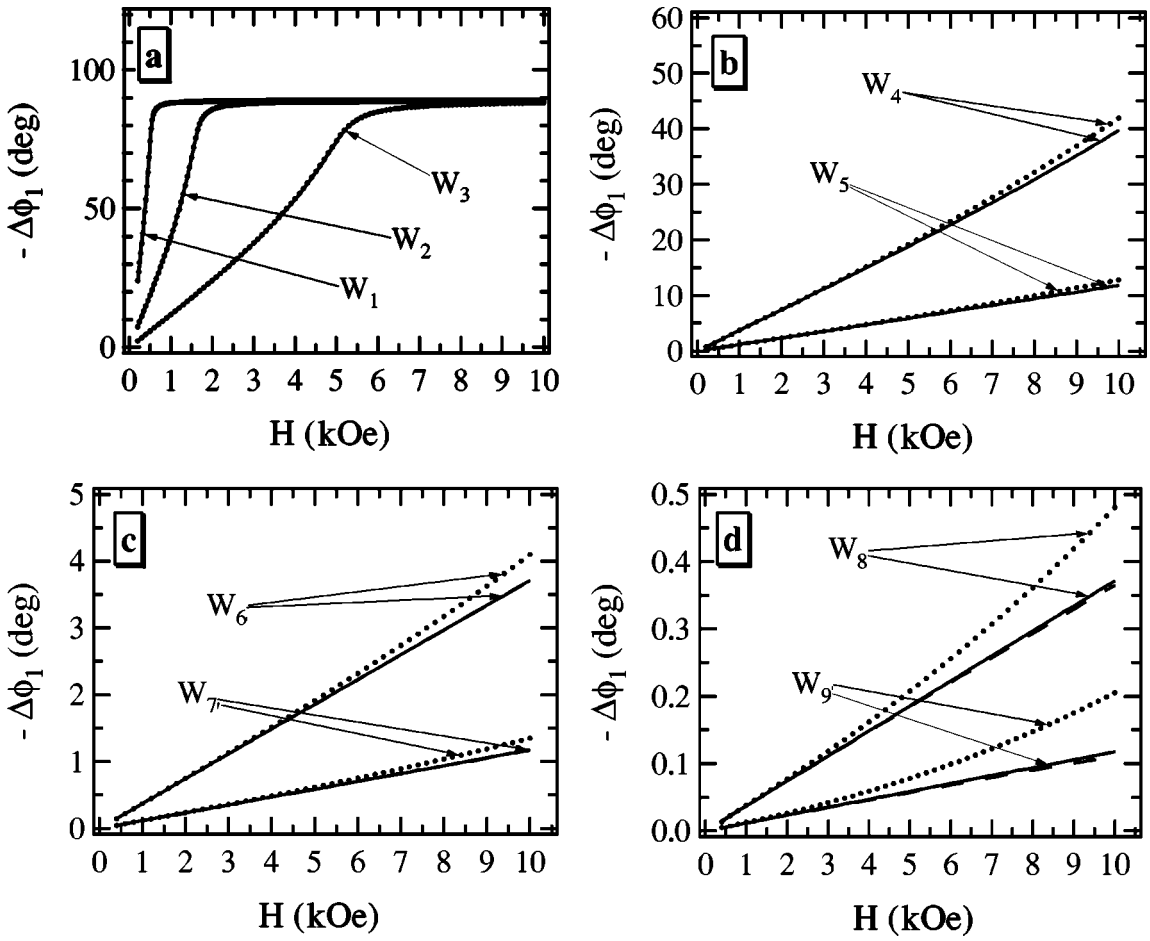


FIG. 8. Rotation angle $\Delta\phi_1$ of the director at surface 1 as a function of intensity $H$ of the magnetic field in the case of method I. On the vertical axis of Figs. 8(a–d) is shown the opposite of $\Delta\phi_1$, which corresponds to difference $\phi_e-\phi_1$ between the azimuthal easy angle and the actual director azimuthal angle. Points represent the values of $\Delta\phi_1$ obtained using the approximate relation $\Delta\phi_1=\Delta\beta/2$. The full curves correspond to the true surface director rotation $\Delta\phi_1$, while the broken curves represent the surface rotation which is obtained using relation $\Delta\phi_1=\Delta\beta/2-\Delta\phi_{app}$, where $\Delta\phi_{app}$ is the value of the apparent surface rotation calculated using the analytical expressions (A8) and (A9) given in Appendix A with the numerical coefficients in Table I. Apart from Fig. 8(d) (very strong anchoring energies), the broken and full curves appear to be superimposed. Different figures [(a), (b), (c), and (d)] and different curves refer to the different values of the azimuthal anchoring energy coefficient: $W_1=10^{-4}$ erg/cm$^2$, $W_2=3.16\times10^{-4}$ erg/cm$^2$, $W_3=10^{-3}$ erg/cm$^2$, $W_4=3.16\times10^{-3}$ erg/cm$^2$, $W_5=10^{-2}$ erg/cm$^2$, $W_6=3.16\times10^{-2}$ erg/cm$^2$, $W_7=10^{-1}$ erg/cm$^2$, $W_8=3.16\times10^{-1}$ erg/cm$^2$ and $W_9=1$ erg/cm$^2$. All the numerical data have been obtained for the surface azimuthal angle at surface 1, $\phi_e=89°$ and for $\phi_2=0°$. The other parameters characterizing the NLC and the substrate are the same as in Fig. 3.

fact, in a real experiment, the accuracy of the measurement of the azimuthal anchoring energy coefficient depends also on the accuracy on the measurement of phase coefficient $\beta$. Many accurate experimental techniques have been developed in the past to measure the phase coefficient of an oscillating signal. A maximum accuracy of the order of 0.01° can be reached with these methods. If the anchoring is very strong [$W=W_9=1$ erg/cm$^2$ in Fig. 8(d)], the surface director rotation in the linear portion of the $\Delta\phi_1(H)$ curve corresponds to very small values of $\Delta\phi_1$ ($\Delta\phi_1<0.02°$) that are comparable to the experimental uncertainty on the measurement of the optical phase shift $\Delta\beta$. In such a special case, it seems to be convenient to extend the experimental measurements to the high magnetic field region also, where the surface director rotations are large enough but the nonlinear contribution $\Delta\phi_{app}$ is no more completely negligible. Also, in this case, it is possible to avoid errors due to the nonadiabatic contributions using the slightly more complicated procedure outlined below. In fact, in this region of still small surface rotations [see Fig. 8(d)], $\Delta\phi_1$ is accurately represented by a linear function of $H$ [Eq. (49)], while the spurious contributions are quadratic in $H$. The main contribution to the spurious rotation $\Delta\phi_{app}$ is given in Eq. (36), which can be rewritten in the compact form

$$\Delta\phi_{app}=b_2H^2\sin(2\phi_1), \tag{50}$$

where $b_2$ is a constant coefficient. Let $\phi_e$ be the azimuthal easy angle at surface 1. For small surface director rotations ($|\Delta\phi_1|\ll1$ rad), Eq. (50) becomes

$$\Delta\phi_{app}\approx b_2H^2\sin(2\phi_e)+2b_2H^2\cos(2\phi_e)\Delta\phi_1. \tag{51}$$

TABLE I. $a_{21}(i)$, $a_{41}(i)$, $a_{42}(i)$, and $a_{43}(i)$ expressed in degrees corresponding to the adimensional coefficients defined in Eq. (A9) in the case of method I.

| | $a_{21}(i)$ | $a_{41}(i)$ | $a_{42}(i)$ | $a_{43}(i)$ |
|---|---|---|---|---|
| $i=1$ | −57.079 | 45.745 | 25.406 | 157.38 |
| $i=2$ | −5.1174 | 42.335 | −76.340 | 297.14 |
| $i=3$ | 12.148 | −143.56 | 262.82 | −1008.5 |
| $i=4$ | 6.3125 | −53.913 | 98.030 | −375.15 |
| $i=5$ | 161.93 | −1423.2 | 2647.5 | −10152 |
| $i=6$ | 35.904 | −623.86 | 1194.8 | −4351.5 |
| $i=7$ | 26.704 | −424.33 | 796.62 | −2889.6 |
| $i=8$ | 36.471 | −178.45 | 307.46 | −1285.8 |
| $i=9$ | −69.105 | 539.91 | −1005.5 | 3907.7 |
| $i=10$ | −19.767 | 243.27 | −459.82 | 1711.8 |

Substituting $\Delta\phi_1$ given in Eq. (49) into Eq. (51), we get

$$\Delta\phi_{app} \approx B_2 H^2 + C_2 H^3, \tag{52}$$

where $B_2$ and $C_2$ are constant coefficients. Then, the magnetic-field dependence of the experimental phase shift $-\Delta\beta/2 = -\Delta\phi_1 - \Delta\phi_{app}$ is

$$-\Delta\beta/2 \approx A_2 H - B_2 H^2 - C_2 H^3, \tag{53}$$

where only coefficient $A_2$ is related to the true surface rotation. Therefore, the true surface rotation and the anchoring energy coefficient can be obtained from a cubic polynomial fit of the experimental values of $-\Delta\beta/2$ versus the magnetic field intensity $H$. Coefficient $A_2 = \sqrt{K_{22}\chi_a}/W$ of the linear term provides a measurement of the anchoring energy coefficient. Note that also in this case, no knowlege of the material and geometric parameters of the NLC is needed to obtain coefficient $A_2$.

An example of this procedure is shown in Fig. 9. Points in Fig. 9 correspond to the numerical values of $\Delta\beta/2$ obtained for an anchoring energy $W=1$ erg/cm$^2$. The full line represents the best fit with Eq. (53). The anchoring energy coefficient is obtained from the best fit coefficient $A_2$ using the simple relation $W = \sqrt{K_{22}\chi_a}/A_2$. The anchoring energy coefficient, which is obtained from the best fit, is $W = 1.0025$ erg/cm$^2$ in a very good agreement with the actual value $W=1$ erg/cm$^2$. In conclusion, very strong anchoring energies can also be accurately measured using the transmission light methods proposed in this paper. It is important to emphasize here that no knowledge of the material parameters of the nematic LC and of the substrate is needed to obtain coefficient $A_2$. The analysis above was focused on method I, but the same kind of results are also obtained in the case of method II.

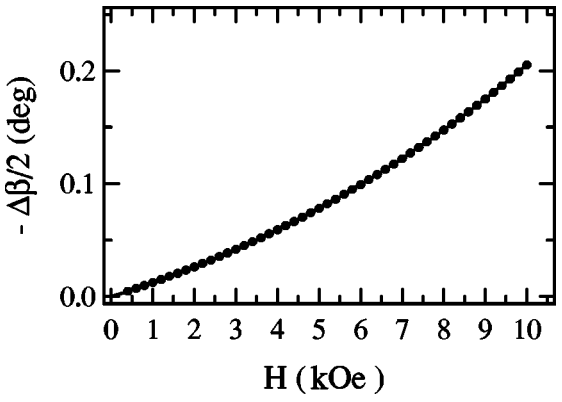


FIG. 9. Points denote the optical phase shift $-\Delta\beta/2$ vs the magnetic field intensity $H$ for an anchoring energy coefficient $W=1$ erg/cm$^2$ (strong anchoring). The full line corresponds to the best fit with the cubic function in Eq. (53).

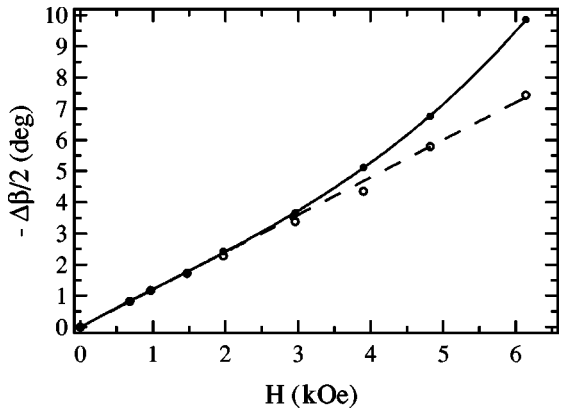


FIG. 10. Preliminary experimental results obtained using method II with the nematic liquid crystal 5CB at temperature $T=34.8$ °C. The substrate is a thin obliquely evaporated SiO layer. Full points correspond to the experimental values of $-\Delta\beta/2$ obtained with method II. Open points are the surface rotation angle $-\Delta\phi_1$, as measured using the reflectometric method given in Ref. [16]. The broken line is the linear fit made on the first three full points. The full line represents the fit with Eq. (53).

To verify the theoretical results obtained in this paper, we have performed a preliminary experiment (see Fig. 10) using method II. The 5CB nematic sample was introduced by capillarity (in the isotropic phase) within a cell made of two glass plates. Then, the sample was cooled toward the anisotropic phase. The glass plates were separated by two mylar spacers having thickness $d_1=80$ $\mu$m and $d_2=200$ $\mu$m, placed at a distance of 5 mm to produce a wedge angle $\theta_W = 1.4°$. The surfaces of the plates in contact with the NLC were treated by oblique evaporation of SiO at 60° to induce a planar homogeneous alignment along the same directions on the two plates. A laser beam impinged at the center of the cell, where the local thickness was $d=140$ $\mu$m.

Here, we are also interested in showing that the nonlinear fitting procedure proposed above (Fig. 9) works well in the case where the spurious director rotation is not negligible. For this reason, we have chosen experimental conditions where the nonadiabatic contributions are appreciable. In particular, we have set the surface easy angle $\phi_e = 78°$ which is far from the optimal condition $\phi_e = 90°$ where nonlinear contributions vanish. Furthermore, we used temperature $T = 34.8$ °C, which is close to the clearing temperature $T_c = 35.3$ °C, in order to have a small value of $\Delta n$ and thus, a great value of $\alpha$. The maximum value $\alpha = 0.31$ was reached at the maximum magnetic field $H=6.14$ kOe. Black points

in Fig. 10 show the experimental phase shift $-\Delta\beta/2$ versus the intensity of the applied magnetic field, while open points correspond to the values of the surface director rotation $-\Delta\phi_1$ which is obtained with a reflectometric method developed by our group in the past [16]. This latter reflectometric method is virtually insensitive to the effects of the bulk director twist [14] but it is more sensitive to external noise sources as those caused by the light diffusion from the NLC. Within the experimental accuracy of the present measurement ($\simeq 0.1°$), the two measurements (transmitted light and reflected light) lead to the same linear behavior in the low magnetic field region (full and open points are virtually superimposed in Fig. 10 for $H<1.5$ kOe). The linear fit on the first three full points in Fig. 10 leads to the broken line which corresponds to the anchoring energy coefficient $W=(5.5\pm 0.3)10^{-3}$ erg/cm$^2$, while the linear fit of the reflectometric results (open points) led to $W=(5.7\pm 0.3)10^{-3}$ erg/cm$^2$. The values of $W$ are calculated using parameters $K_{22}=1.92\times 10^{-7}$ dyn [22] and $\chi_a=0.71\times 10^{-7}$ [23]. The full line in Fig. 10 represents the best fit with Eq. (53). From coefficient $A_2$ of this nonlinear fit, we recover value $W=\sqrt{K_{22}\chi_a}/A_2=(5.5\pm 0.3)10^{-3}$ erg/cm$^2$ which was obtained from the measurements restricted to the linear region. Therefore, the validity of the nonlinear fitting procedure is fully confirmed by the experiment. Of course, in the case of Fig. 10, the surface director rotation in the low magnetic fields region is sufficiently high and the use of the nonlinear fitting procedure is not useful. According to the previous theoretical analysis, the nonlinear behavior, which is present in the transmission light, results (full points) can be greatly reduced by setting the easy angle close to 90°. This behavior is effectively confirmed in our experiment.

Before terminating this section we want to emphasize that most of expressions given in this paper have been obtained in the case of a semi-infinite nematic sample. However, the proposed experimental methods can also be applied to the cases where the characteristic length $\xi$ of the director distortion is not much smaller than the local thickness $d$ of the nematic sample. In such a case, the higher order perturbative contributions are usually negligible and the surface director angle is accurately obtained using equality $\phi_1=\beta/2$. Now, a little more complicated expressions have to be used to calculate the anchoring energy from the measured rotation of the director at the surface.

## VI. CONCLUSIONS

The transmission of a monochromatic beam by a twisted nematic liquid crystal subjected to a magnetic field has been investigated in detail, using both a perturbative approach and a numerical analysis. It has been shown that there exist two special geometric arrangements (method I and method II) that allow one to obtain an accurate measurement of the director orientation at the surface, from the measurement of phase coefficient $\beta$ of the transmitted light intensity. In these special geometries, the surface azimuthal angle $\phi_1$ is related to $\beta$ by the simple relation

$$\phi_1=\beta/2, \tag{54}$$

up to the second order in the perturbative parameter $\alpha=1/(\Delta k\xi)$. Furthermore, the small residual higher order contributions vanish if the director at surface 1 is oriented orthogonal to the magnetic field. Then, the influence of these spurious contributions can be greatly reduced by setting the easy axis at surface 1 almost orthogonal to the magnetic field. The experimental procedure is very simple and direct and needs only a standard measurement of phase shift of an oscillating signal. This procedure makes it possible to improve greatly the accuracy attainable with the classical transmitted light methods. In particular, it is also possible to measure strong anchoring energies ($W\approx 1$ erg/cm$^2$) with a satisfactory accuracy. The great simplicity and accuracy of these methods make them a valid alternative to the more complex reflectometric methods too.

The two methods proposed here to measure the anchoring energy are virtually equivalent, but method I is very sensitive to the orientation of the easy axis on the second interface, which must be $\phi_2=0°$. A small misalignment of the director on the second interface introduces spurious contributions (see Fig. 3) that are indistinguishable from those due to the anchoring mechanism, because they exhibit the same linear dependence on the applied magnetic field. Furthermore, this method uses an analyzer with the transmission axis which must be set parallel to the director at surface 2. Therefore, a great care must be devoted to the alignment procedures when method I is used. On the contrary, method II is virtually insensitive to the orientation of the director field on the second interface and does not requires the use of an analyzer. In particular, method II can also be applied successfully to a symmetric cell having the same easy axes on both the interfaces (the preliminary experimental results given above were just obtained in this geometric condition). This latter technique requires only that a nematic wedge is built with a wedge angle $\theta_W>1°$, sufficient to separate appreciably the refracted ordinary and extraordinary beams. For all these reasons we think that method II should be preferred.

## ACKNOWLEDGMENT

We acknowledge financial support by the European Community (INTAS Grant: 01-0170).

## APPENDIX A: HIGHER ORDER CONTRIBUTIONS IN METHOD I

In this appendix we will restrict our attention to the special case of a semi-infinite nematic layer with $\phi_2=0°$ and we will disregard the small residual dependence of the apparent surface director rotation $\Delta\phi_{app}$ on $\delta$. In such a case, according to the numerical results given in Sec. III B, the apparent rotation $\Delta\phi_{app}$ is well represented by the expression

$$\Delta\Phi_{app}=a_2\alpha^2+a_4\alpha^4, \tag{A1}$$

where $a_2$ and $a_4$ are the coefficients that depend only on the azimuthal angle $\phi_1$ at surface 1 and on the refractive indices of the NLC ($n_e$ and $n_o$) and of the substrate ($n$). According to the perturbative analysis given in Sec. III A, $\Delta\phi_{app}$ is

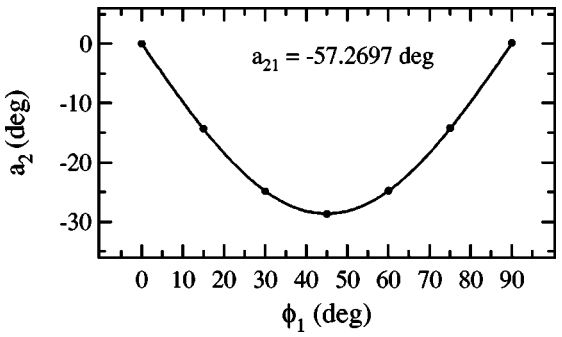


FIG. 11. Points represent the values of the adimensional coefficient $a_2$ of Eq. (A1) versus the $\phi_1$-angle for $\phi_2=0°$ (method I). Coefficient $a_2$ has been obtained from the best fits in Fig. 4. The full line represents the best fit with Eq. (A6). The material and geometric parameters of the NLC layer are the same as in Fig. 3.

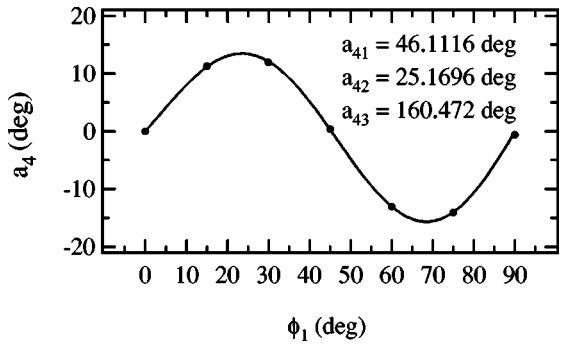


FIG. 12. Points represent the values of coefficient $a_4$ of Eq. (A1) vs the $\phi_1$ angle for $\phi_2=0°$ (method I). Coefficient $a_4$ has been obtained from the best fits in Fig. 4. The full line represents the best fit with Eq. (A7). The material and geometric parameters of the nematic liquid crystal layer are the same as in Fig. 3.

expected to depend essentially on the values of the derivatives of the director azimuthal angle at the first interface and on $1/(\Delta k)=\lambda/(2\pi\Delta n)$ [see Eq. (10)]. For simplicity, we will denote here these surface derivatives with symbols $\phi_1'$, $\phi_1''$, $\phi_1'''$, $\phi_1^{IV}$, and so on. For a semi-infinite NLC ($d\gg\xi$), the first four surface derivatives are:

$$\phi_1'=-\frac{\sin\phi_1}{\xi}, \tag{A2}$$

$$\phi_1''=\frac{1}{\xi^2}\frac{\sin 2\phi_1}{2}, \tag{A3}$$

$$\phi_1'''=-\frac{1}{\xi^3}\cos 2\phi_1 \sin\phi_1, \tag{A4}$$

$$\phi_1^{IV}=\frac{1}{\xi^4}\left[-2\sin 2\phi_1 \sin^2\phi_1+\frac{\sin 4\phi_1}{4}\right]. \tag{A5}$$

According to the analysis given in Sec. III A , the apparent director rotation $\Delta\phi_{app}$ is only due to the higher order perturbative contributions in $\alpha$. The quadratic correction $a_2\alpha^2$ in Eq. (A1) is expected to be derived from the sum of contributions that are proportional to $\phi'^2$ and to $\phi''$. However, we find that the contribution proportional to $\phi'^2$ is completely negligible. Then, coefficient $a_2$ can be written as

$$a_2=a_{21}\frac{\sin 2\phi_1}{2}, \tag{A6}$$

where $a_{21}$ is an adimensional numerical coefficient which depends only on the refractive indices of the NLC and of the substrate.

Points in Fig. 11 represent the numerical values of coefficient $a_2$ versus $\phi_1$. The full line in Fig. 11 is the best fit of the numerical data with the function in Eq. (A6). Then, the second order corrections to the Mauguin regime are proportional to the second derivative of the director azimuthal angle and vanish for $\phi_1=0°$ and $\phi_1=90°$. The fourth order corrective contributions $a_4\alpha^4$ in Eq. (A1) are expected to depend on $\phi_1^{IV}$, $(\phi_1'')^2$, $\phi_1''(\phi_1')^2$, $\phi_1'\phi_1'''$, and $(\phi_1')^4$. However, our numerical analysis shows that the first three contributions are sufficient to describe accurately the observed behavior. Then, $a_4$ can be written in the general form as

$$a_4=a_{41}\left[-2\sin 2\phi_1 \sin^2\phi_1+\frac{\sin 4\phi_1}{4}\right]+a_{42}\frac{\sin^2 2\phi_1}{4}+a_{43}\frac{\sin 2\phi_1}{2}\sin^2\phi_1, \tag{A7}$$

where $a_{41}$, $a_{42}$, and $a_{43}$ are adimensional coefficients that depend only on the refractive indices of the NLC and of the substrate. Figure 12 shows the dependence of $a_4$ on $\phi_1$ and the corresponding best fit with the function in Eq. (A7). In this case too, coefficient $a_4$ reduces to zero at $\phi_1=0°$ and $\phi_1=90°$. In conclusion, a satisfactory analytical approximation to $\Delta\Phi_{app}$ is given by:

$$\Delta\phi_{app}=a_{21}\frac{1}{(\Delta k\xi)^2}\frac{\sin(2\phi_1)}{2}+\frac{1}{(\Delta k\xi)^4}\left\{a_{41}\left[\frac{\sin(4\phi_1)}{4}-2\sin(2\phi_1)\sin^2\phi_1\right]+a_{42}\left[\frac{\sin(2\phi_1)}{4}\right]^2+a_{43}\frac{\sin 2\phi_1}{2}\sin^2\phi_1\right\}. \tag{A8}$$

Coefficients $a_{21},\ldots,a_{43}$ in Eq. (A8) depend on the refractive indices of the NLC and of the substrate. To obtain a suitable analytical approximate expression for this dependence, we have repeated many (625) calculations of coefficients $a_2$ and $a_4$ in Eq. (A1), changing the ordinary refractive index $n_o$, the optical anisotropy $\Delta n=n_e-n_o$, refractive index $n$ of the substrate, and the surface angle $\phi_1$. Coefficients $a_2$ and $a_4$ were obtained from the best fits of $\Delta\phi_{app}$ with the function in Eq. (A1) for $\alpha<0.28$ ($\alpha<0.28$ corresponds to $H<10$ kOe for the NLC 5CB at room temperature). Once $a_2$ and $a_4$ were known, $a_{21}$, $a_{41}$, $a_{42}$, and $a_{43}$ were obtained from the best fits of $a_2$ and $a_4$ with the functions in Eqs. (A6) and (A7). The investigated intervals of

refractive indices were $1.4<n_o<1.6$, $0.07<\Delta n<0.28$, and $1.4<n<1.7$, which represent the typical values for standard liquid crystals and substrates. Let $n_o^m=1.5$, $\Delta n^m=0.175$, and $n^m=1.5$ be the average values of $n_o$, $\Delta n$, and $n$ in each interval and $\delta n_o=n_o-n_o^m$, $\delta\Delta n=\Delta n-\Delta n^m$, and $\delta n=n-n^m$. We find that a satisfactory analytical approximated form for functions $a_{ij}(n_o,\Delta n,n)$ in this restricted region of material parameters is given by the following quadratic expression:

$$a_{ij}=a_{ij}(1)+a_{ij}(2)\,\delta n_o+a_{ij}(3)\,\delta\Delta n+a_{ij}(4)\,\delta n+a_{ij}(5)\,\delta n_o\delta\Delta n+a_{ij}(6)\,\delta n_o\delta n+a_{ij}(7)\,\delta\Delta n\,\delta n+a_{ij}(8)\,\delta n_o^2+a_{ij}(9)\,\delta\Delta n^2+a_{ij}(10)\,\delta n^2. \quad \text{(A9)}$$

Coefficients $a_{ij}(k)$, obtained by the best fits of the numerical values of $a_{21}$, $a_{41}$, $a_{42}$, and $a_{43}$ with Eq. (A9), are reported in Table I.

Then, a suitable approximated value of $\Delta\phi_{app}$ can be obtained by using the analytical expression in Eq. (A8) with $a_{21}$, $a_{41}$, $a_{42}$, and $a_{43}$ given by Eq. (A9) and with $a_{ij}(k)$ in Table I. We have verified that the values of $\Delta\phi_{app}$, which are obtained using this procedure, coincide within 0.1° with the "exact" ones in the whole range of parameters ($1.4<n_o<1.6$, $0.07<\Delta n<0.28$, $1.4<n<1.7$, $\alpha<0.28$, and $0<\phi_1<90$). This uncertainty (0.1°) is greatly reduced for low magnetic fields ($\alpha\ll 0.28$). Note that the main contribution to $\Delta\phi_{app}$ comes from the first quadratic term ($a_{21}$). Neglecting the fourth order terms ($a_{41}$, $a_{42}$, and $a_{43}$) produces a maximum error of 0.04° at the maximum magnetic field ($\alpha\approx 0.28$) in the whole range of material parameters investigated here.

## APPENDIX B: NUMERICAL METHOD TO OBTAIN THE AMPLITUDE OF THE EXTRAORDINARY WAVE

In this appendix we describe briefly the numerical method used to extract the amplitude of the generalized extraordinary wave from the numerical results obtained using the Berreman approach.

We consider a plane nematic layer of thickness $d$. If the reflections at the interfaces are disregarded, the amplitude of the transmitted beam is expected to be given by the sum of the two waves that propagate with the ordinary and extraordinary phase velocities. In this case, the amplitude of the transmitted beam is reduced to the simple form in Eq. (18). In the more general case, where multiple reflections cannot be disregarded, the output amplitude will be the superposition of a lot of different contributions. Here we consider only two adjunctive contributions coming from the extraordinary and ordinary beams, which are reflected two times from the interfaces of the nematic sample. With this assumption, the amplitude of the transmitted electric field is

$$\mathbf{E}^{out}=\mathbf{E}_e^{out}\exp(i\,\delta_e)+\mathbf{E}_o^{out}\exp(i\,\delta_o)+\mathbf{E}_{re}^{out}\exp(i3\,\delta_e)+\mathbf{E}_{ro}^{out}\exp(i3\,\delta_o). \quad \text{(B1)}$$

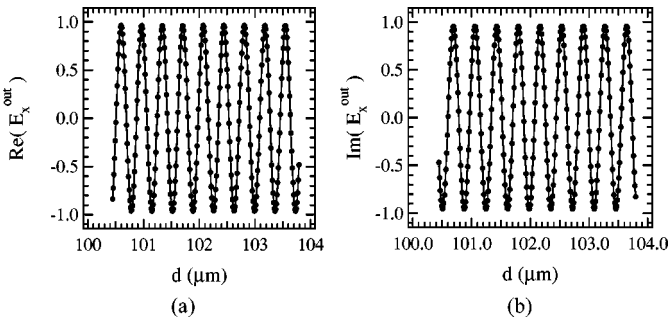


FIG. 13. Points denote the real [Fig. 13(a)] and imaginary [Fig. 13(b)] parts of the $x$ component of the complex output amplitude $\mathbf{E}^{out}$ of the electromagnetic wave versus thickness $d$ of the nematic layer for a magnetic field of amplitude $H=10$ kOe. The full curves are obtained by substituting in Eq. (B1) the numerical values of $\mathbf{E}_e^{out}$, $\mathbf{E}_o^{out}$, $\mathbf{E}_{re}^{out}$, and $\mathbf{E}_{ro}^{out}$ obtained with the procedure discussed in this appendix. The surface director angles are $\phi_1=45°$ and $\phi_2=0°$. The material parameters are the same as in Fig. 3. The maximum relative difference between the two calculated values is 0.02%.

$\mathbf{E}_e^{out}$ and $\mathbf{E}_o^{out}$ are the amplitudes of the beams that are never reflected by the interfaces, while $\mathbf{E}_{re}^{out}$ and $\mathbf{E}_{ro}^{out}$ are the amplitudes of the beams that are reflected two times at the interfaces of the NLC (the nematic wedge spatially separates all these different terms). The numerical Berreman procedure allows us to directly calculate only the total output amplitude $\mathbf{E}^{out}$. In order to obtain amplitude $\mathbf{E}_e^{out}$ of the extraordinary beam which is not reflected from the interfaces, we calculate amplitudes $\mathbf{E}_1^{out}$, $\mathbf{E}_2^{out}$, $\mathbf{E}_3^{out}$, and $\mathbf{E}_4^{out}$, which correspond to four different values $d_1$, $d_2$, $d_3$, and $d_4$ of thickness $d$. Then, by exploiting Eq. (B1) we obtain a linear system of four equations in the four unknowns $\mathbf{E}_e^{out}$, $\mathbf{E}_o^{out}$, $\mathbf{E}_{re}^{out}$, and $\mathbf{E}_{ro}^{out}$, which is numerically solved. In Figs. 13(a,b), the thickness dependence of the real and imaginary parts of the $x$ component of $\mathbf{E}^{out}$ are shown. Points in Figs. 13(a,b) represent the numerical values of $\mathrm{Re}(E_x^{out})$ and $\mathrm{Im}(E_x^{out})$, while the full lines correspond to the result obtained by substituting in Eq. (B1) the numerical values of $\mathbf{E}_e^{out}$, $\mathbf{E}_o^{out}$, $\mathbf{E}_{re}^{out}$, and $\mathbf{E}_{ro}^{out}$ obtained with the procedure discussed above. The very good

TABLE II. $a_{21}(i)$, $a_{41}(i)$, $a_{42}(i)$, and $a_{43}(i)$ expressed in degrees corresponding to the adimensional coefficients defined in Eq. (A9) in the case of method II.

| | $a_{21}(i)$ | $a_{41}(i)$ | $a_{42}(i)$ | $a_{43}(i)$ |
|---|---|---|---|---|
| $i=1$ | −57.479 | 49.480 | 18.346 | 184.30 |
| $i=2$ | −5.9545 | 36.895 | −62.914 | 256.52 |
| $i=3$ | −9.8385 | 79.428 | −156.43 | 565.55 |
| $i=4$ | 0.92966 | 0.065852 | −2.4163 | 5.3930 |
| $i=5$ | 15.806 | −350.81 | 697.82 | −2497.7 |
| $i=6$ | −43.920 | 449.87 | −838.72 | 3173.4 |
| $i=7$ | −64.450 | 666.72 | −1252.6 | 4748.3 |
| $i=8$ | −62.567 | 338.32 | −580.00 | 2440.6 |
| $i=9$ | 55.428 | −511.85 | 976.55 | −3673.8 |
| $i=10$ | 9.9531 | −86.703 | 161.90 | −619.00 |

agreement between the two sets of data confirms that Eq. (B1) represents satisfactorily the actual optical behavior.

## APPENDIX C: HIGHER ORDER CONTRIBUTIONS IN METHOD II

In this appendix we report detailed results concerning the dependence of the higher order corrections to the adiabatic theorem in the case of method II. To calculate the higher order correction terms, we restrict our attention to case $\phi_2 = 0°$. In such a case, the director orientation at interface 2 does not change when the magnetic field is switched on. However, it has to be noted that the higher order corrections are poorly dependent on angle $\phi_2$ in the case of method II. Using the same procedure described in Appendix A , we can obtain a satisfactory analytical approximated form of the kind in Eq. (A8) for the apparent rotation $\Delta\phi_{app}$. The values of coefficients $a_{21}$, $a_{41}$, $a_{42}$, and $a_{43}$ are obtained using Eq. (A9) in the same ranges of values of $n_o$, $\Delta n$, $n$, and $\alpha$, as in Appendix A. The numerical values of coefficients $a_{ij}(k)$, obtained with this procedure are given in Table II.

The maximum uncertainty on the numerical values of $\Delta\phi_{app}$, which are obtained using the numerical coefficients in Table II, is lower than 0.15° in the whole range of investigated material parameters and reduces to less than 0.01° for magnetic fields lower than 3 kOe.


[1] P.G. de Gennes, *The Physics of Liquid Crystals* (Clarendon, Oxford, 1974).

[2] S. Faetti, in *Physics of Liquid Crystalline Materials*, edited by I.C. Khoo and F. Simoni (Gordon and Breach, New York, 1991).

[3] J. Sicart, J. Phys. (Paris), Lett. **37**, L25 (1976).

[4] H.A. van Sprang, J. Phys. (Paris), Lett. **44**, 421 (1983).

[5] G. Barbero, E. Miraldi, C. Oldano, M.L. Rastrello, and P.T. Valabrega, J. Phys. (Paris), Lett. **4**, 1411 (1986).

[6] P. Allia, C. Oldano, and T. Trossi, Mol. Cryst. Liq. Cryst. **143**, 17 (1987).

[7] P. Allia, C. Oldano, and T. Trossi, Phys. Scr. **37**, 755 (1988).

[8] T. Oh Ide, S. Kuniyasu, and S. Kobayashi, Mol. Cryst. Liq. Cryst. **164**, 91 (1988).

[9] S. Faetti and C. Lazzari, J. Appl. Phys. **71**, 3204 (1992).

[10] E. Polossat and I. Dozov, Mol. Cryst. Liq. Cryst. Sci. Technol., Sect. A **282**, 223 (1996).

[11] D. Adrienko, A. Dyadyusha, A. Iljin, Yu. Kurioz, and Yu. Reznikov, Mol. Cryst. Liq. Cryst. Sci. Technol., Sect. A **321**, 271 (1998).

[12] V. Vorflusev, H. Kitezerow, and V. Chigrinov, Jpn. J. Appl. Phys., Part 1 **34**, L1137 (1995).

[13] T. Akahane, H. Kaneko, and M. Kimura, Jpn. J. Appl. Phys., Part 1 **35**, 4434 (1996).

[14] S. Faetti, V. Palleschi, and A. Schirone, Nuovo Cimento Soc. Ital. Fis. **10D**, 1313 (1988).

[15] S. Faetti, M. Nobili, and A. Schirone, Liq. Cryst. **10**, 95 (1991).

[16] S. Faetti and M. Nobili, Liq. Cryst. **25**, 487 (1998).

[17] D.W. Berreman, J. Opt. Soc. Am. **62**, 502 (1972).

[18] Equations (8) and (9) are slightly different from those given in Ref. [5]. The correctness of Eqs. (8) and (9) is confirmed by the comparison with our numerical results obtained with the Berreman method (see Sec. III B). For sufficiently small values of $\alpha$, the numerical results and those predicted by Eqs. (8) and (9) are the same within 0.5%. This small discrepancy is due to the effects of reflections from the interfaces that are disregarded in the perturbative approach.

[19] J.W. Goodman, *Introduction to the Fourier Optic* (McGraw-Hill, New York, 1968).

[20] A. Rapini and M. Papoular, J. Phys. (Paris), Colloq. **30**, C4-54 (1969).

[21] M. Nobili, C. Lazzari, A. Schirone, and S. Faetti, Mol. Cryst. Liq. Cryst. Sci. Technol., Sect. A **212**, 97 (1992).

[22] T. Toyooka, G. Chen, H. Takezoe, and A. Fukuda, Jpn. J. Appl. Phys., Part 1 **26**, 1959 (1987).

[23] P.L. Scherrel and D.A. Crellin, J. Phys. Colloq. **40**, C3-213 (1979).

[24] P.P. Karat and N.V. Madhusudana, Mol. Cryst. Liq. Cryst. **36**, 51 (1976).